Traffic WILEY

Golgi screen identifies the RhoGEF Solo as a novel regulator of RhoB and endocytic transport

Cristiana Lungu[1,2] | Florian Meyer[1] | Marcel Hörning[2,3] | Jasmin Steudle[1] |
Anja Braun[1] | Bettina Noll[1,2] | David Benz[1] | Felix Fränkle[1] |
Simone Schmid[1] | Stephan A. Eisler[1,2] | Monilola A. Olayioye[1,2]

[1]Institute of Cell Biology and Immunology, University of Stuttgart, Stuttgart, Germany

[2]Stuttgart Research Center Systems Biology (SRCSB), University of Stuttgart, Stuttgart, Germany

[3]Institute of Biomaterials and Biomolecular Systems, Biobased Materials Group, University of Stuttgart, Stuttgart, Germany

Correspondence
Monilola A. Olayioye, Institute of Cell Biology and Immunology, University of Stuttgart, Allmandring 31, 70569 Stuttgart, Germany.
Email: monilola.olayioye@izi.uni-stuttgart.de

Abstract

The control of intracellular membrane trafficking by Rho GTPases is central to cellular homeostasis. How specific guanine nucleotide exchange factors and GTPase-activating proteins locally balance GTPase activation in this process is nevertheless largely unclear. By performing a microscopy-based RNAi screen, we here identify the RhoGEF protein Solo as a functional counterplayer of DLC3, a RhoGAP protein with established roles in membrane trafficking. Biochemical, imaging and optogenetics assays further uncover Solo as a novel regulator of endosomal RhoB. Remarkably, we find that Solo and DLC3 control not only the activity, but also total protein levels of RhoB in an antagonistic manner. Together, the results of our study uncover the first functionally connected RhoGAP-RhoGEF pair at endomembranes, placing Solo and DLC3 at the core of endocytic trafficking.

KEYWORDS
EGFR, endosome, golgi, imaging screen, OptoGEF, optogenetics, RhoB, RhoGAP, RhoGEF

1 | INTRODUCTION

Intracellular trafficking relies on a tight cooperation between cytoskeletal elements, proteins and lipids that come together to regulate cellular homeostasis.[1–3] While the contribution of the small GTPases of the Rab and Arf families to membrane trafficking is well established, the involvement of Rho GTPases in this process is less understood. Since aberrant membrane trafficking is known to be associated with various diseases including cancer, it is important to elucidate the molecular mechanisms underlying the control of Rho GTPase signalling at different target membranes.

Rho GTPases function as molecular switches cycling between an active GTP-bound state and an inactive GDP-bound state. RhoGEFs promote the exchange of bound GDP for GTP, leading to Rho activation and initiation of downstream signalling pathways. RhoGAPs promote the low intrinsic GTP hydrolysis activity of the Rho GTPase, thereby dampening downstream signalling.[4,5] In addition to the plasma membrane, active Rho GTPase pools are also found at endomembranes such as endosomes and the Golgi complex.[2,3] For example, RhoB is detected at endosomes from where it controls the recycling of cargoes such as the epidermal growth factor receptor (EGFR).[3,6,7] Notably, RhoB pools localized at the plasma membrane and endosomes appear to be functionally distinct, the latter playing the main role in EGFR recycling.[7] Additionally, RhoB and RhoA are important for the architecture of the Golgi complex, their hyperactivation causing severe fragmentation of this organelle.[8] With 145 members, the RhoGEF and RhoGAP proteins greatly exceed the 10 classical Rho family GTPase switch proteins.[2,9–11] This complexity underscores the need for unbiased approaches to identify and characterize GEFs and GAPs co-regulating Rho GTPase signalling in distinct cellular contexts.

Among the RhoGAP proteins, the Deleted in Liver Cancer (DLC) family stands out, being deregulated in different cancer types more frequently than any other Rho regulator.[12,13] DLC3, also known as STARD8, is the least characterized member of the DLC family.[10] Work from our lab has uncovered a RhoGAP-specific function of DLC3 in the maintenance of the integrity of the Golgi complex and the endocytic recycling compartment.[14,15] Furthermore, in HeLa cells, DLC3 partially co-localized with endosomal RhoB and regulated trafficking in a RhoA/B dependent manner.[14] The RhoGEF counterpart of DLC3 responsible for Rho activation at endomembranes has nevertheless remained elusive to date.

By performing an image-based RNAi screen using the morphology of the Golgi complex as a readout, we here identify the RhoGEF protein Solo, also known as ARHGEF40 or Scambio, as an antagonist of cellular DLC3 activity. Subcellular fractionation, imaging and optogenetic recruitment experiments further revealed Solo to be present on a subset of RhoB-positive endosomes, where it can locally activate this GTPase. In addition to activity, we unexpectedly find that Solo and DLC3 co-regulate RhoB protein levels. Together, the results of our study uncover the first functionally connected RhoGAP-RhoGEF pair at endomembranes, placing Solo and DLC3 at the core of RhoB regulation and endocytic trafficking.

2 | METHODS

2.1 | Cell culture

HEK293T and HeLa cells (ATCC) were cultured in RPMI 1640 (Invitrogen) supplemented with 10% foetal calf serum (FCS; PAA Laboratories). The cells were maintained in a humidified incubator at 37°C with 5% CO_2. All cell lines were authenticated, tested negative for Mycoplasma (Lonza, LT07-318) and were kept in culture for no longer than 2 months.

2.2 | Antibodies and reagents

Following primary antibodies were used for detection: anti-AKT (Cell Signalling Technology, Cat# 2920), anti-Phospho-(Thr308)-AKT (Cell Signalling Technology, Cat# 2965), anti-Calnexin (Cell Signalling Technology, Cat# 2433), anti- EEA1 (Cell Signalling Technology, Cat# 3288), anti-EGFR (Santa Cruz, Cat# sc-03-G), anti-EGFR (Santa Cruz, Cat# sc-101), anti-Phospho-(Tyr1068)-EGFR (Cell Signalling Technology, Cat# 3777), anti-p44/42 MAPK (Erk1/2) (Cell Signalling Technology, Cat# 9107), anti-Phospho-(Thr202/Tyr204) p44/42 MAPK (Erk1/2) (Cell Signalling Technology, Cat# 9101), anti-GAPDH (Sigma-Aldrich, Cat# G9545), anti-GFP (Cell Signalling Technology, Cat# 2956), anti-Giantin (Abcam, Cat# 37266), anti-GST (GE Healthcare, Cat# 27457701), anti-HA (Sigma-Aldrich, Cat# 11867423001), anti-Rab5 (Cell Signalling Technology, Cat# 3547), anti-Rab7 (Cell Signalling Technology, Cat# 9367), anti-RhoA (Santa Cruz, Cat# sc-418), anti-RhoB (Santa Cruz, Cat# sc-8048, used for western bloting), anti-RhoB (Cell Signalling Technology, Cat# 2098, used for microscopy), anti-

RhoC (Cell Signalling Technology, Cat# 3430), anti-Solo (custom made, Pineda Antibody Service, Berlin).

HRP-labelled secondary anti-mouse-IgG, anti-rabbit-IgG and anti-goat-IgG were purchased from Dianova (Cat# 115-035-062, Cat# 111-035-144, Cat# 705-035-147). Alexa-Fluor®-labelled secondary IgG antibodies, Alexa-Fluor®-labelled phalloidin and TO-PRO-3 were obtained from Invitrogen. DAPI was obtained from Sigma-Aldrich.

2.3 | Generation of a polyclonal anti-Solo antibody by rabbit immunization

Protein epitope analyses including sequence comparisons were carried out to avoid cross-reactivity. The selected peptide (1015–1032aa of human ARHGEF40, isoform 1, UniProtKB Q8TER5–1) was synthesized and separated by HPLC for subsequent immunization of three rabbits (Pineda Antibody-Service). The pre-immune and resulting immunization sera were analysed by western blotting, periodically over a total time span of 3 months, which included monthly rounds of immunization. To compare the quality, specificity and affinity of the sera collected from the three animals, lysates of HeLa cells with either Solo overexpression or Solo knockdown were used (see Figure S2B). The IgG fraction of the antibody generated was separated by affinity chromatography (Pineda Antibody-Service) and aliquots were stored at −80°C for subsequent use.

2.4 | RNA interference and plasmid transfection

For transient knockdowns, the cells were transfected using Lipofectamine™ RNAiMAX (Invitrogen) according to manufacturer's instructions. The cells were used for experiments at 48–72 h post transfection as described in the figure legends. The siRNAs used were: negative control siRNA (siNT, ON-TARGETplus® non-targeting control pool D-001810-10 from Dharmacon), siDLC3sp (siGENOME SMARTpool human STARD8 M-010254 from Dharmacon), siDLC3ss (Silencer® Select STARD8 s18826 from ThermoFisher Scientific), siARHGEF2sp (ON-TARGETplus® SMARTpool, L-009883), siARHGEF2ss (Silencer® Select ARHGEF2, 4392420 from ThermoFisher Scientific) siRhoBsp (ON-TARGETplus® SMARTpool RhoB L-008395 from ThermoFisher Scientific), siRhoBss (Silencer® Select RHOB, 4427037 from ThermoFisher Scientific), siSolo ss#2 (Silencer® Select ARHGEF40 s31288 from ThermoFisher Scientific) and siSolo sp#4 (ON-TARGETplus Human ARHGEF40 siRNA J-030269-12 from Dharmacon). siRNAs sequences of the RhoGEF library are provided in Table S1. For plasmid transfections of HeLa and HEK293T cells, LipofectamineLTX (ThermoFisher Scientific) and TransIT-293 (Mirus) regents, respectively, were used according to manufacturer's instructions.

2.5 | RNAi Golgi screen and analysis

The RhoGEF screen was performed using a WiScan Hermes High content imaging system (Idea Biomedical). To this end, 5×10^4 HeLa cells were seeded per well in CollagenR coated glass bottom 96-well plates

(Greiner). The cells were subjected to reverse transfection using 2.5 pmol siRNA consisting of siDLC3sp and siRhoGEF or siNT control mixed at a 1: 1 ratio. 72 h post-transfection, the cells were washed with PBS, fixed and stained for the Golgi complex (Giantin, Alexa Fluor® 488, green channel) and the nuclei (TO-PRO-3, far red channel) as described in the immunofluorescence staining section. Images were acquired with the high resolution 40× 0.75 NA objective for green and red channels. Per well, a coverage of 85% and a field density of 20% was applied, resulting in 200 frames. Images were analysed with the implemented WiSoft Minerva analysis application development platform: In brief, nuclei and Golgi complexes were segmented using the corresponding channels. Cells were segmented related to nuclei and Golgi compartments using the cytoplasmic background signal of the Golgi staining. To increase the accuracy, cells touching the image edge, mitotic cells and cells with oversegmented nuclei were excluded from the analysis. The number and average perimeter of Golgi fragments were measured per cell in order to quantify the state of Golgi fragmentation. The screen was performed twice.

For statistical analysis, the number of Golgi vesicles and average perimeter of Golgi vesicles a log-transformation was applied, as the data show a Poisson distribution and strongly skewed normal distribution, respectively. The mean $\mu_{\log}$ and standard deviation $\sigma_{\log}$ were calculated from the log-transformed data

$$X_{\log} = \log(X),$$

as

$$\mu_{\log} = \frac{1}{N}\sum_{i=1}^{N} X_{\log}^i,$$

$$\sigma_{\log} = \sqrt{\frac{1}{N}\sum_{i=1}^{N}\left(X_{\log}^i - \mu_{\log}\right)^2},$$

and back-transformed to obtain the mean and variance in normal space as

$$\mu = e^{\mu_{\log} + 0.5\sigma_{\log}^2},$$

$$\sigma^2 = \mu^2\left(e^{\sigma_{\log}^2} - 1\right),$$

following the Finney estimator approach.[16]

The data were statistically analysed using a N-way ANOVA (NANOVA) method in Matlab (Mathworks, R2021a). The two p-values obtained from the two screenings were combined as:

$$p_{ij} = \frac{\left(w_{s1}\,p_{ij}^{s1} + w_{s2}\,p_{ij}^{s2}\right)}{\sqrt{w_{s1}^2 + w_{s2}^2}},$$

with the two weights

$$w_{s1,2} = \frac{N_{s1,2}}{N_{s1} + N_{s2}},$$

where N is the relative number of observables at each screening.

The Golgi screen dataset (Table S3) is available from the University of Stuttgart at: https://darus.uni-stuttgart.de/privateurl.xhtml?token=e0aa3f7b-ac8c-4253-8eb4-c8ae826346eb. The combined p values of the Golgi screen analysis are provided in Figure S1—figure supplement 2B.

2.6 | DNA constructs

The GEF inactivating L1217E Solo point mutation was introduced by QuickChange site directed mutagenesis using pIRESNEO-Scambio-HA (Addgene plasmid #33354) as a template and the following forward and reverse primers: 5′- CTCGGTATGGGCGGGAGCTGGAGGAGCTCCTG -3′ and 5′- CAGGAGCTCCTCCAGCTCCCGCCCATACCGAG -3′. QuickChange site directed mutagenesis was also used to generate the RhoB Q63L (5′- GTGGGACACAGCTGGCCTGGAGGACTAC GACCGC -3′ and 5′- GCGGTCGTAGTCCTCCAGGCCAGCTGTGTCC CAC -3′) and the RhoB T19N variant (5′- GATGGAGCCTGTGGAAA GAACTGCTTGCTCATAGTCTTC -3′ and 5′- GAAGACTATGAGCAAG CAGTTCTTTCCACAGGCTCCATC -3′) using the pEGFP-C1-RhoB plasmid as a template. The Opto-Endo Solo-GEF plasmid was generated by Gibson assembly whereby the coding sequence of PLD (Endosome-targeted optoPLD[17]) was exchanged for the Solo DHPH GEF domain (aa1076–aa1380) amplified using the following primers: 5′- CGATCG GGCGGATCTATGGAGCGCAAGCGAAGC -3′ and 5′- GTTTGTAGCGCC GCTTCCCTCCTTGTTGTGGGCTGCC -3′. Solo GEF domain borders were selected following the approach previously used to generate the ARHGEF11 DHPH GEF domain.[18] All constructs were validated by Sanger sequencing. The pCRV62-Met-Flag-DLC3 WT, mCherry-DLC3 K725E, pEGFP-C1-RhoB plasmids were previously described.[14,15,19] Endosome-targeted optoPLD was a gift from Jeremy Baskin (Addgene plasmid # 140056[17]). pEGFP-C1-Anillin AHPH WT and A70D/E758K (DM) were provided by Alpha Yap (University of Queensland).[20,21] pcDNA™3.1 was from Invitrogen.

2.7 | Quantitative real-time PCR

Total RNA was isolated using the NucleoSpin® RNA Kit (Macherey-Nagel) according to manufacturer's instructions. 100 ng RNA were used for real-time PCR with the Power SYBR® Green RNA-to-C$_T$™ 1-Step kit (Applied Biosystems) and the CFX96 Touch Real-Time PCR Detection System (Bio-RAD, 1855196). Changes in gene expression levels were determined relative to the housekeeping gene RPLP0 (5′- CTCTGCATTCTCGCTTCCTGGAG -3′ and 5′- CAGATGGATCAGC CAAGAAGG -3′) using the $2^{-\Delta\Delta Ct}$ method. Hs_ARHGEF40_1_SG and Hs_STARD8_1_SG QuantiTect Primer Assays (Qiagen) were used to detect the *ARHGEF40* and the *STARD8* transcripts, respectively.

The 5′- CATTCTGACCACACTTGTACGC -3′ and 5′- GGTTTCTTTT CCCTCTCC TTGT -3′ primers were used for *RHOB*.

2.8 | Cell lysis, SDS-PAGE and western blotting

Cells were washed with PBS and harvested by scraping in ice-cold lysis buffer (150 mM Tris-HCl pH 7.5, 500 mM NaCl, 1% [v/v] Triton X-100, 0.5% [v/v] sodium deoxycholate, 0.1% [w/v] SDS, 10% Glycerol [v/v], 10 mM MgCl$_2$, 1 mM DTT, 1 mM sodium orthovanadate, 10 mM sodium fluoride, 0.5 mM PMSF, 20 mM β-glycerophosphate and cOmplete™, EDTA-free Protease Inhibitor Cocktail [Roche]). The cell lysates were passed five times through a 27-gauge needle, followed by 20 min incubation on ice. Subsequently, the whole-cell lysate was clarified by centrifugation for 10 min at 16000 g and 4°C. The protein concentration of the supernatant was determined by performing a DC protein assay (Bio-rad). Equal protein amounts were separated by SDS-PAGE (NuPage® Novex® 4%–12% Bis-Tris gels, Invitrogen) and transferred to nitrocellulose membranes using an iBlot® device (iBlot®Gel Transfer Stacks; Invitrogen). The membranes were blocked with 0.5% (v/v) blocking reagent (Roche) in PBS containing 0.05% (v/v) Tween-20 and 0.01% (v/v) Thimerosal and then incubated with primary antibodies, overnight at 4°C, followed by 1 h incubation with HRP-conjugated secondary antibodies at room temperature. The chemiluminescence signal was detected using an AmershamTM Imager 600 device (GE Healthcare) followed by quantification of the 16-bit images in the linear range using the inbuilt ImageQuant TL 8.1 software.

For inhibitor experiments, HeLa cells were treated with either 30 mM NH$_4$Cl (Carl Roth) or 5 μM MG132 (Selleck Chemicals) for 12 h before harvesting. Cycloheximide (Calbiochem) was used for the indicated time points at a concentration of 50 μg/ml.

2.9 | RBD pulldowns

BL21—CodonPlus competent cells (Agilent Technologies) were transformed with a plasmid encoding the GST-tagged domain of Rhotekin (Addgene plasmid # 15247). Cells were cultivated in Terrific broth medium at 37°C while shaking until an OD (600 nm) of 0.6–0.7 was reached. Then, protein expression was induced by addition of 1 mM of isopropyl-β-D-thiogalactoside and the culture was incubated at 21°C shaking at 200 rpm for another 16 h. The cells were harvested by centrifugation at 4°C (15 min at 4600 rpm) and the pellet resuspended in sonication buffer (50 mM Tris-HCl pH 7.5, 500 mM NaCl, 1 mM DTT, 5 mM MgCl$_2$, 10% glycerol, cOmplete™, EDTA-free Protease Inhibitor Cocktail [Roche]). The cells were lysed by sonication and centrifuged at 18 000 rpm for 1 h to prepare a clear lysate, which was applied on a GST-sepharose column (GE Healthcare). After washing with sonication buffer, the protein was eluted with sonication buffer containing 50 mM reduced glutathione (Sigma-Aldrich) and dialyzed against storage buffer (50 mM Tris-HCl pH 7.5, 150 mM NaCl, 1 mM DTT, 5 mM MgCl$_2$, 10% glycerol) for 3 h. The eluted protein was aliquoted and stored at −80°C till further use.

For pulldowns, cells were stimulated with 100 ng/ml EGF for 5 min, washed once with cold TBS (50 mM Tris-HCl pH 7.6, 140 mM NaCl) and lysed in ice-cold RBD lysis buffer (150 mM Tris-HCl pH 7.5, 500 mM NaCl, 1% [v/v] Triton X-100, 0.1% [w/v] SDS, 0.5% sodium deoxycholate [v/v], 1 mM DTT, 10% Glycerol [v/v], 10 mM MgCl$_2$, 1 mM EGTA, 1 mM sodium orthovanadate, 10 mM sodium fluoride, 0.5 mM PMSF, 20 mM β-glycerophosphate and cOmplete™, EDTA-free Protease Inhibitor Cocktail [Roche]). The cell lysate was passed 5 times through a 27-gauge needle, followed by centrifugation for 5 min at 16 000 g and 4°C. Equal amounts of cleared lysates were incubated for 45 min at 4°C with 30 μg GST–RBD protein pre-bound to GST-sepharose beads. Beads were rapidly washed four times with RBD lysis buffer, the eluted proteins were separated by SDS-PAGE and analysed by western blotting as described above.

2.10 | Immunofluorescence staining and confocal microscopy

Cells grown on glass coverslips coated with 10 μg/ml collagen R (Serva) were fixed for 15 min with 4% (w/v) paraformaldehyde. After washing with PBS supplemented with Ca^{2+} and Mg^{2+}, the cells were incubated for 15 min with 150 mM glycine in PBS followed by permeabilization for 5 min with 0.1% (v/v) Triton X-100 in PBS. Blocking was performed with 5% (v/v) goat serum (Invitrogen) in PBS containing 0.1% (v/v) Tween-20. Fixed cells were incubated with primary antibodies diluted in blocking buffer overnight at 4°C. Following three washing steps with PBS, the cells were then incubated with Alexa-Fluor®-(488, 546 or 633)-labelled secondary antibodies in blocking buffer for 1 h at room temperature. For the immunolabelling of endogenous RhoB, the method by Adamson et al.[6] was followed. In short, after fixation and permeabilization, cells were incubated with 10% FCS in PBS for 30 min, followed by incubation overnight at 4°C with the anti-RhoB antibody (Santa Cruz, Cat# sc-8048) diluted 1:100 in incubation buffer (50 mM Tris-HCl, pH 7.6, 1% NP-40, 0.5% sodium deoxycholate and 5 mM EDTA), which was also used for washing and dilution of the secondary antibody. Nuclei were counterstained with DAPI and the coverslips were mounted in Molecular Probes™ ProLong™ Gold Antifade mountant (ThermoFisher Scientific).

All samples were analysed at room temperature using a confocal laser scanning microscope (LSM 710 or LSM 980 Airyscan 2, Carl Zeiss) equipped with a Plan Apochromat 63×/1.40 DIC M27 (Carl Zeiss) oil-immersion objective. The excitation wavelengths and detection window used were as follows: 405 nm and 425–488 nm for DAPI; 488 nm and 496–544 nm for GFP and Alexa-Fluor®-488 coupled probes; 561 nm and 573–621 nm for mCherry and Alexa-Fluor®-546 coupled probes; 633 nm and 650–717 nm for Alexa-Fluor®-633 coupled probes. All images were acquired with the pinhole of each channel adjusted to the same optical slice thickness. Linear adjustments to brightness, contrast and maximum intensity projections were made using the ZEN software (Carl Zeiss). Fluorescence intensities along a line of interest were measured using the ZEN software. The Manders' coefficient was determined using the JACoP plugin.[22]

2.11 | Live cell imaging of GFP-DLC3 and mCherry-DLC3 K725E

HeLa cells were seeded onto collagen-coated 35 mm high glass bottom μ-Dishes (ibidi, cat. no: 81158) followed by transient transfection with the plasmids of interest as described in the RNA interference and transfection section above. Twenty-four hours later, the cells were imaged on a Zeiss Cell Observer SD Spinning Disk microscope equipped with an EMCCD camera (Photometrics Evolve 512). GFP was visualized with a 488 nm diode laser in combination with a FE01-520/35 nm emission filter. mCherry was visualized with a 561 nm diode laser in combination with a 600_50 ET emission filter. Images were acquired at 37°C and 5% CO_2 every 20 s for a time interval of 10 min. Image processing was done with Zen 2.3 blue software.

2.12 | Setup of optogenetics experiments used to validate the OptoEndo-Solo-GEF tool

Samples were illuminated with 405 nm light in a custom-made box equipped with six equally spaced high-power 3W LEDs 700 mA. Illumination cycles were 5 sec on − 35 sec off. Following 90 cycles of illumination, cells were fixed with 4% (w/v) paraformaldehyde. This was followed by permeabilization for 5 min with 0.1% (v/v) Saponin in PBS before immunofluorescence staining for EEA1, as described above. Dark control samples were not exposed to light and were fixed directly after being taken out of the incubator.

2.13 | Setup and analysis of live cell imaging optogenetics experiments

HeLa cells were seeded onto collagen-coated 35 mm high glass bottom μ-Dishes (ibidi, cat. no: 81158). After 48 h, cells were transfected with 1.75 μg total plasmid DNA mixture consisting of 0.6 μg OptoEndo-Solo-GEF, 0.25 μg pEGFPC1-AHPH and 0.65 μg pcDNA3. The cells were imaged 6 h post transfection. For knockdown experiments, the cells were reverse transfected with RhoB siRNA 48–72 h before transfection with plasmid DNA. Images were acquired every 20 s on an LSM910 Airyscan (Carl Zeiss) instrument equipped with a Plan-Apochromat 63×/1.4 Oil DIC objective and an environment control chamber. The excitation wavelengths and detection window used were 488 nm and 499–549 nm for GFP and 561 nm and 573–627 nm for mCherry, respectively. For imaging, only cells with weak basal mCherry fluorescence were selected. While identifying pEGFPC1-AHPH double transfected cells, the exposure time to the 488 nm laser was kept to a minimum. Several imaging dishes were prepared in parallel for each condition to avoid unintentional optogenetic recruitment of OptoEndo-Solo-GEF outside of the acquisition timeframes.

To identify and follow single endosomes, the plugin TrackMate[23] was employed. To this end, .czi files were imported into Fiji using Bio-Formats[24] and the LoG detector was used to detect individual endosomes in the pre-processed (median) mCherry channel. The expected vesicle diameter was set to 0.7 μm and the quality threshold to 50. To ensure that the detected endosomes are linked correctly during tracking, the linking max distance was set to 1.5 μm and the gap closing max distance/max frame gap to 0. To ensure that the detected endosomes are linked correctly during tracking, the linking max distance was set to 1.5 μm and the gap closing max distance/max frame gap to 0. Based on the determined track-ID as well as x- and y-coordinates further steps were performed.

The analysis pipeline consisted of three steps. First, the TrackMate data was filtered for endosomes, which were detected in the five consecutive frames $t = 14$ to $t = 19$ (1:20 min). To reduce the amount of data that has to be processed for each endosome, a 1.4 μm × 1.4 μm ROI for each frame was generated, the middle of the endosome and therefore mCherry signal being centred. Additionally, a circular median filter was applied to both channels. Next, thresholds were determined and set. To take differences in the expression level of the GFP-AHPH probe into account, a cell-specific GFP threshold was determined. For this, GFP pixel intensity values of all endosome ROIs were collected, the median and SD calculated, and the GFP threshold set to 'median $+ 1×$ SD' value. In addition, each endosome received its own mCherry threshold value. Since the mCherry signal was centred, the pixel intensities of the middle $5 × 5$ px square were collected for the frames of the endosome. Based on this, the threshold was defined as the 'minimum value $− 0.15×$ minimum value' to allow fluctuations. After thresholding, every endosome but the centred one were excluded to prevent false-positive overlap. Finally, the positive endosomes were determined. If the thresholded mCherry and GFP pixels overlapped to any extent throughout the defined timespan, the endosome track was defined as positive. The amount of positive endosomes was subsequently divided by the total amount of endosomes to define the relative GFP-AHPH enrichment at OptoEndo-Solo GEF per cell. All calculations were done using an in house written Python script.

2.14 | EGFR trafficking and signalling assays

For immunofluorescence analysis of EGFR trafficking, HeLa cells were starved for 20 h in RPMI supplemented with 0.5% serum before stimulation with 10 ng/ml EGF. The cells were then washed with PBS, fixed, blocked in 5% (v/v) goat serum in PBS and incubated with an antibody recognizing the extracellular domain of EGFR (Santa Cruz, Cat# sc-101). This was followed by permeabilization as described above and incubation with an antibody recognizing the C-terminus of EGFR (Santa Cruz, Cat# sc-03-G). Cells used for EGFR signalling analysis were treated in a similar manner before being lysed in ice-cold RIPA buffer (50 mM Tris-HCl pH 7.5, 150 mM NaCl, 1% [v/v] NP-40, 0.1% [w/v] SDS, 0.25% sodium deoxycholate [v/v], 1 mM EDTA, 1 mM sodium orthovanadate, 10 mM sodium fluoride, 0.5 mM PMSF, 20 mM β-glycerophosphate and cOmplete™, EDTA-free Protease Inhibitor Cocktail [Roche]) and processed for western blot analysis.

2.15 | Statistical analysis

Data are presented as mean + SEM, where each experiment, apart from the Golgi screen, was performed at least three times. The Golgi screen was performed twice. For box plots, the box represents the 25–75th percentiles, and the median is indicated; whiskers extend 1.5 times the interquartile range from the 25th and 75th percentiles, and outliers are represented as determined by GraphPad Prism 7 software. 'N' refers to the number of sample points and 'n' to the number of independent experiments. Significance between multiple groups was determined by one-way ANOVA followed by Tukey (all vs. all) or Dunnett (all vs. control) multiple comparison post-test, as detailed in the figure legends. The two-way ANOVA analysis was followed by Sidak post-testing. Significance between two groups was determined by *t*-test. Data were analysed using GraphPad Prism 7. *p* Values: *$*p \leq 0.03$; **$p \leq 0.002$; ***$p \leq 0.0002$; ****$p \leq 0.0001$, n.s.: non-significant. See also Table S2.

3 | RESULTS

3.1 | RhoGEF screen identifies Solo as a potential DLC3 antagonist

We previously found that DLC3 controls the integrity of the Golgi and endocytic recycling compartments in a RhoA/B dependent
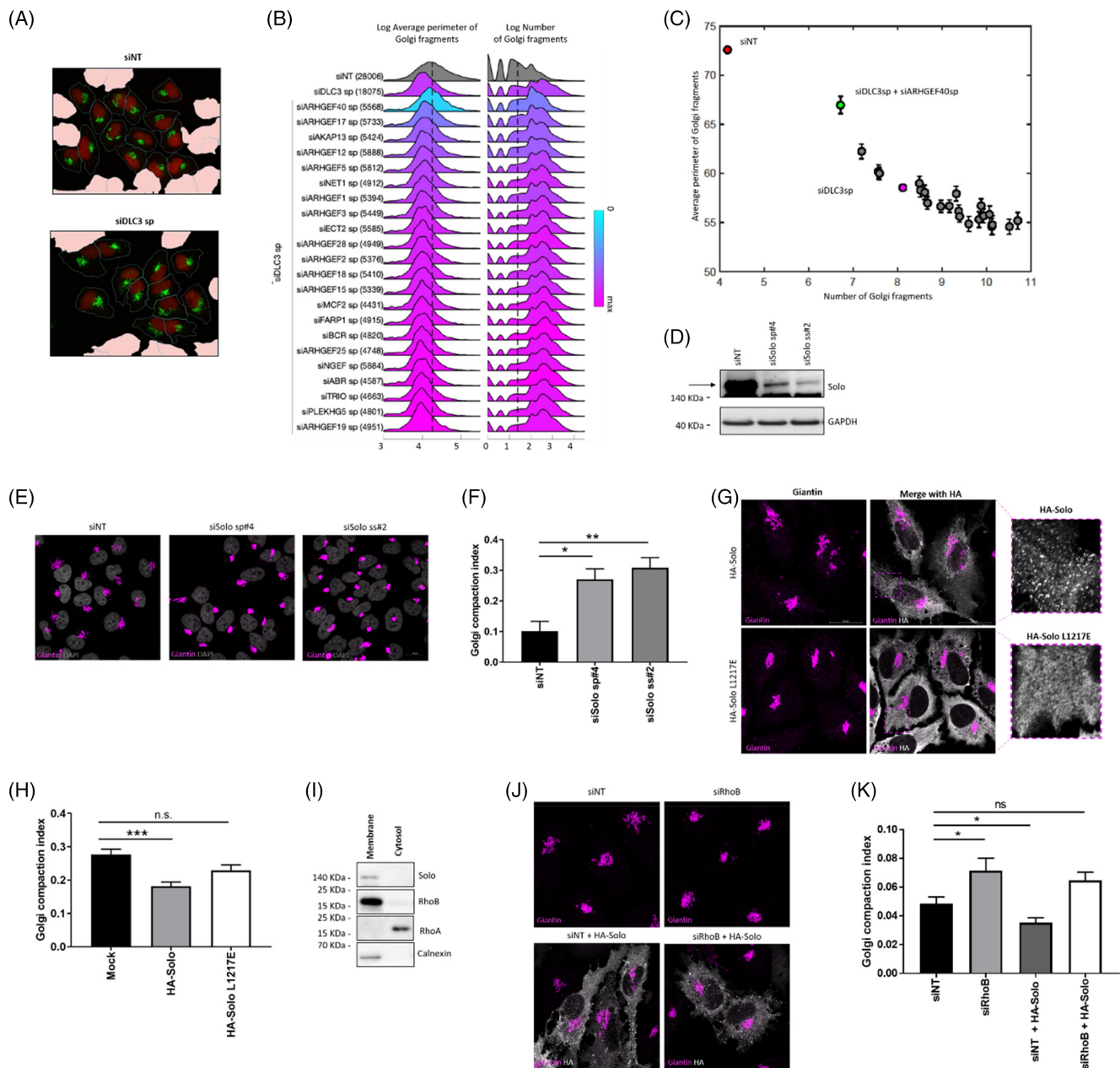

FIGURE 1 Legend on next page.

manner.[14] Since the structure of the Golgi is sensitive to cytoskeletal remodelling and membrane trafficking,[25,26] we used the morphology of this organelle as a general readout to screen for antagonists of DLC3 function. Twenty-three GEF proteins with known in vitro, and in many cases, also in vivo specificity for the RhoA/B/C subfamily of GTPases were tested. To this end, HeLa cells were transiently transfected with Smartpool siRNAs specific for the individual RhoGEFs along with DLC3-specific siRNA, followed by automated image analysis of immunostained cells. Labelling of the Golgi and the nucleus were used to identify and segment the cells of interest as well as to detect outliers (Figure S1—figure supplement 1—A and B). The morphological features of the Golgi complex, for example, the number and average perimeter of Golgi fragments (Figure 1B,C) were then computed. In accordance with our previous work,[14] DLC3 knockdown cells displayed a doubling of the number of giantin-positive fragments per cell and a significant decrease in the average perimeter of the Golgi fragments (Figure 1A–C and Figure S1—figure supplement 2B). Remarkably, whereas the knockdown of most of the RhoGEF proteins had little effect on the number and the average perimeter of Golgi fragments in DLC3-depleted cells, the knockdown of the RhoGEF Solo (ARHGEF40) stood out for its ability to bring the compact structure of the Golgi complex closest to the control cells (Figure 1B,C; Figure S1—figure supplement 1C and Figure S1—figure supplement 2).

This rescue was not because of a decrease in DLC3 knockdown efficiency upon simultaneous depletion of Solo (Figure S1—figure supplement 1D).

3.2 | Solo is required for the integrity of the Golgi complex in a RhoGEF-dependent manner

To validate Solo as a regulator of Golgi complex morphology, we depleted the transcript using two independent siRNAs and confirmed the efficient knockdown at the RNA (Figure S1—figure supplement 3A) and protein level using a Solo-specific antibody generated in-house (Figure 1D; Figure S1—figure supplement 3B). For both siRNAs, Solo knockdown led to a significant increase in the Golgi compaction index, without affecting total cell area (Figure 1E,F; Figure S1—figure supplement 1E and F). To investigate if Golgi morphology changes are direct and depend on Solo GEF activity, we transfected HeLa cells with plasmids encoding either the wild-type protein or a GEF inactive Solo mutant.[28] Only the expression of wild-type Solo led to a significant fragmentation of the Golgi complex showing that Solo GEF activity is essential for this phenotype (Figure 1G,H).

While under our conditions, Solo was not enriched at the Golgi, we observed that the wild type protein was localized at vesicles.

FIGURE 1 Imaging-based Golgi screen identifies the RhoGEF Solo as a potential DLC3 antagonist. (A–C) HeLa cells were transfected with control (siNT), DLC3-specific, or a combination of DLC3 and RhoGEF specific smartpool siRNAs. 72 h post transfection, cells were fixed, stained and scanned with the Hermes WiScan. Images were analysed with WiSoft. (A) Representative fluorescence microscopy images of control and siDLC3 cells used to establish the image analysis pipeline for the RhoGEF screen. Shown are segmented HeLa cells fixed and stained for the Golgi complex (green) and nucleus (red) at 72 h post transient knockdown with the indicated siRNAs. DLC3 depleted cells display a fragmented Golgi complex. (B) Quantification of the morphology of the Golgi complex for the RhoGEF screen performed as described above. Shown are the log average perimeter of Golgi vesicles (left panel) and the number of Golgi fragments (right panel). The number of cells used for analysis is annotated in parenthesis for each siRNA transfection set. The colour scheme indicates the differences between the means of the control (siNT) and the respective knockdown. Simultaneous depletion of ARHGEF40 (=Solo), brings the Golgi complex morphology of DLC3sp cells closest to the siNT control. Statistical parameters, e.g. mean and variance, were obtained by log-transformation using the Finney estimator approach. (C) The relation between the number and the average perimeter of Golgi vesicles: Error bars = 95% confidence intervals. Data points highlighted in colour are the control (siNT, red), siDLC3sp (pink) and siDLC3sp + siARHGEF40sp (green) cells. Data were statistically analysed using the N-way ANOVA (NANOVA) method in Matlab. See also the histograms of the number and average perimeter of each respective siRNA transfection (Figure S1—figure supplement 2A) and the p-value matrix for the specific statistical comparisons performed for each screen (Figure S1—figure supplement 2B). (D) Validation of the siRNAs used for Solo knockdown. HeLa cells were transfected with either control or two independent Solo siRNAs, followed by harvesting at 72 h post transfection. Cell lysates were analysed by immunoblotting with a Solo specific antibody. The band corresponding to Solo is annotated with an arrow. GAPDH was used as loading control. (E) Representative confocal immunofluorescence microscopy images showing the morphology of the Golgi apparatus (Giantin, pink) in HeLa cells 72 h post transfection with either control or Solo specific siRNAs. Nuclei were stained with DAPI (grey). All images were acquired and displayed using identical settings. (F) Quantification of the morphology of the Golgi complex in HeLa cells exemplarily shown in (E) using the Golgi compaction index method.[27] Data show the mean + S.E.M. ($n = 3$, $N \geq 30$ cells). Statistical comparison by one-way ANOVA and Dunnett post-test; *$p \leq 0.03$; **$p \leq 0.002$. (G) Representative confocal immunofluorescence microscopy images documenting the morphology of the Golgi apparatus (Giantin, pink) in HeLa cells 24 h post transient transfection with plasmids encoding either wild type or GEF inactive L1217E HA-Solo (HA, white). All images were acquired using the superresolution modus of the Airyscan microscope and are displayed using identical settings. Scale bars: 20 μm. (H) Quantification of the Golgi morphology in HeLa cells with transient overexpression of wild type and L1217E HA-Solo as shown in (G). Data show the mean + S.E.M. ($n = 3$, $N = 37$–46 cells). The significance of differences was analysed by a one-way ANOVA and Dunnett post-test; ***$p \leq 0.0002$, n.s.: non-significant. (I) HeLa cells were homogenized and fractionated into the membrane and cytosol fractions. Samples were analysed by immunoblotting using the indicated antibodies. (J) Representative confocal immunofluorescence microscopy images documenting the morphology of the Golgi apparatus (Giantin, pink) in HeLa cells 24 h post transient transfection with plasmids encoding HA-Solo (HA, white). 48 h prior to plasmid transfection, the cells were subjected to knockdowns with the indicated siRNAs. All images were acquired and displayed using identical settings. (K) Quantification of the Golgi morphology in transfected HeLa cells as representatively shown in (J). Data show the mean + S.E.M. ($n = 3$, $N = 26$–74 cells). The significance of differences was analysed by a one-way ANOVA and Dunnett post-test; *$p \leq 0.03$, n.s.: non-significant. See also Figure S1—supplement 1–3 and Tables S1–S3

By contrast, the GEF inactive Solo was distributed diffusely throughout the cytoplasm (Figure 1G, crop-ins). Since the Solo antibody did not show a specific signal in immunostainings of HeLa cells, we employed subcellular fractionation to monitor the distribution of endogenous Solo in the cytosolic vs. membrane fraction, containing e.g. endosomes and the plasma membrane[29] (Figure 1I). Calnexin, which was used as a marker for the membrane fraction showed the expected extraction pattern and validated our approach. Interestingly, endogenous Solo was predominantly detected in the membrane fraction together with the small GTPase RhoB but not RhoA. We therefore investigated if RhoB contributes to the Golgi fragmentation phenotype induced by Solo. As shown in Figure 1J,K, depletion of RhoB was sufficient to revert the Golgi phenotype of Solo transfected cells. Together, these findings consolidate the results of the screen and suggest that Solo regulates the morphology of the Golgi through RhoB.

3.3 | Solo activates RhoB on endosomes

A characteristic of small GTPases is to bind to their GEFs in a GDP-bound or nucleotide-free state. By contrast, effectors bind stronger to the GTP-loaded form. Since Solo has not been previously linked to RhoB, we first performed GFP pulldown assays using lysates from HEK293T cell expressing HA-Solo and conformationally locked RhoB-GFP variants (Figure 2A). As anticipated based on its function as a RhoGEF, Solo associated predominantly with the RhoB 19N GDP-locked mutant and less with wild-type RhoB or Q63L RhoB, mimicking the constitutively active protein. No signal was detected for the GFP control, validating the specificity of the interaction. To gain spatial insights into the Solo—RhoB association we next performed immunofluorescence imaging of HeLa cells transiently expressing HA-Solo and GFP-RhoB 19N. In line with previous reports,[30] GDP-locked RhoB localized on vesicles known to be endosomes (Figure 2B). Notably, Solo was detected on a subset of the RhoB 19N positive vesicles (Figure 2D). This colocalization was specific to RhoB, the equivalent RhoA 19N mutant displaying little overlap with Solo (Figure 2C,D). Together with the pulldown results, this finding supports the hypothesis that Solo regulates RhoB activity on endosomes.

To address this hypothesis, we generated OptoEndo-Solo-GEF as a tool to assess the direct activation of endosomal RhoB upon targeted recruitment of the Solo GEF domain. Specifically, in this optogenetic approach, CRY2 was fused to the Solo DHPH-GEF domain and mCherry, while CIBN was fused to the 2×FYVE domain of Hrs1[17] (Figure 2F). The latter recognizes PtdIns(3)P, which is present on the membranes of early and late endosomes.[31] In the absence of blue light, CRY2-Solo-GEF-mCherry displayed a weak mCherry fluorescence, being localized diffusely through the cytoplasm (Figure S2—figure supplement 1A). By contrast, acute illumination resulted in the rapid recruitment of the probe to vesicles, which partially co-localized with the early endosomal marker EEA1 (Figure S2—figure supplement 1A and 1B). To specifically detect Rho-GTP, we co-expressed the GFP-AHPH biosensor.[20,21] Strikingly, OptoEndo-Solo-GEF

recruitment resulted in a significant local enrichment of the GFP-AHPH sensor on endosomes but not of the GFP-AHPH A70D/E758K binding pocket mutant (Figure 2G,H). Of note, this recruitment was dependent on RhoB, because depletion of this GTPase by two independent siRNA mixtures significantly reduced the GFP-AHPH signal at OptoEndo-Solo-GEF endosomes (Figure 2I). Our findings thus show that the GEF activity of Solo regulates RhoB at endosomal membranes.

3.4 | Solo and DLC3 co-regulate RhoB activity and protein levels

We next investigated how the interplay between Solo and DLC3 converges on RhoB by first performing live cell imaging experiments in HeLa cells transiently co-expressing fluorescently tagged Solo and DLC3. To preserve cell morphology, the K725E GAP-inactive DLC3 mutant, which recapitulates the localization of wild-type DLC3, was used.[19] Spinning disk confocal microscopy revealed dynamic co-localization events that occurred between GFP-Solo and mCherry-DLC3 K725E in particular on vesicular-like structures at cell protrusions (Figure 3A,B and Figure S3—figure supplement 1). Unfortunately, while both Solo and DLC3 individually co-localized with RhoB in HeLa cells (Figure 2B),[14] we were not able to detect their co-localization in triple transfection experiments, most likely because of the differential binding of active and inactive forms of RhoB by Solo and DLC3, respectively.

We then used RBD pulldowns to directly assess how endogenous RhoB activity is regulated by Solo and DLC3. Before lysis, the cells were stimulated with EGF, which is a potent RhoB activator.[32] These assays revealed a 40% reduction in the total cellular GTP-RhoB levels (normalized to GAPDH) upon Solo depletion. Intriguingly, this decrease in RhoB-GTP was paralleled by a significant drop in RhoB protein levels (Figure 3D,E), which was not observed for RhoA or RhoC (Figure S3—figure supplement 2A). We also measured RhoB protein levels in HeLa cells depleted of GEFH1, one of the few established GEFs for RhoB.[33] No changes in RhoB amounts were observed under these conditions, indicating that the downregulation of RhoB is specific to Solo and not a general response to global perturbations of RhoB GEF activity (Figure S3—figure supplement 2C). Importantly, simultaneous knockdown of Solo and DLC3 rescued RhoB-GTP as well as total RhoB amounts to levels that were comparable to those of control cells (Figure 3D,E). While normalization of RhoB-GTP to RhoB-GDP amounts showed no net changes in RhoB activity among the different knockdowns (Figure 3F), these results clearly demonstrate that Solo and DLC3 co-regulate RhoB in HeLa cells. These effects were predominantly observed at the post-transcriptional level as qPCR analysis did not reveal significant changes in RhoB transcript levels in response to neither Solo nor DLC3 depletion (Figure 3G).

An intact endosomal trafficking system was found to be required for proper RhoB subcellular localization and the regulation of RhoB stability.[30,34] When visualizing endogenous RhoB using a specific RhoB antibody (Figure S3—figure supplement 2C), we noted that
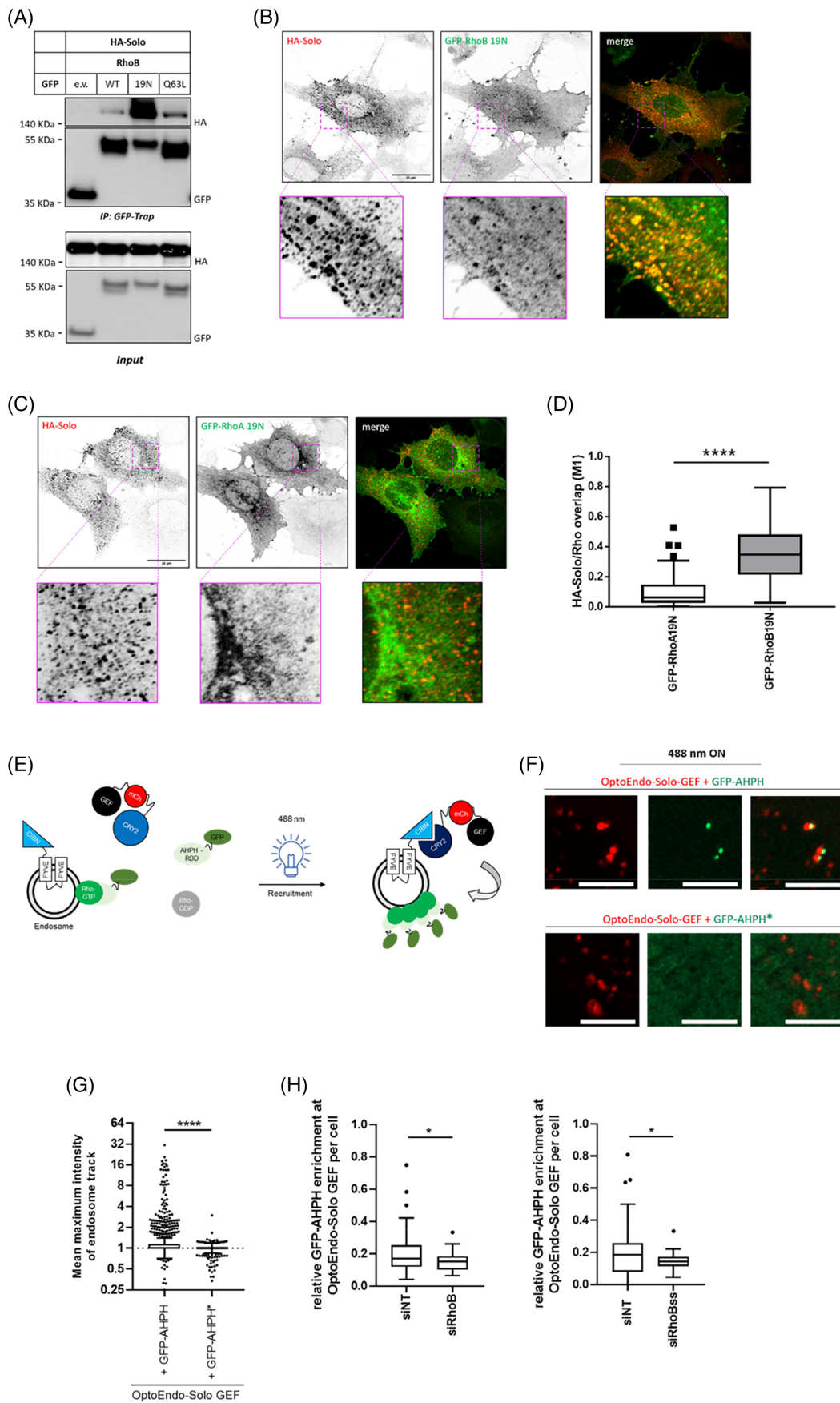
FIGURE 2 Legend on next page.

RhoB was concentrated in the perinuclear area in control cells, while the stabilized RhoB protein also accumulated at the periphery in DLC3 knockdown cells (Figure 4H). Importantly, simultaneous knockdown of Solo not only reduced the increase in RhoB levels observed upon DLC3 depletion, but also led to re-clustering of the GTPase in the perinuclear area as observed for the control cells. This result demonstrates that Solo and DLC3 are required for maintaining the subcellular distribution patterns of RhoB.

To obtain mechanistic insights into the regulation of RhoB protein levels, we next performed cycloheximide chase experiments (Figure S3—figure supplement 3A and 3B). In agreement with measurements in other cell lines,[35,36] RhoB was found to be short-lived in HeLa cells, with a half-life of 2 ± 0.28 h. By contrast, cells with DLC3 knockdown displayed higher RhoB protein stability, with the half-life increased to 8 ± 2.8 h and 5 ± 0.58 h for siDLC3sp and siDLC3ss, respectively. This analysis shows that the increased RhoB levels observed upon DLC3 depletion are attributed to increased protein stability. RhoB was reported to be degraded via both the proteasomal and the endo-lysosomal pathways.[30,37,38] Indeed, treatment with MG132, a proteasomal inhibitor, or NH_4Cl, an inhibitor of lysosomal acidification, increased RhoB levels in control cells (Figure S3—figure supplement 3C). In Solo-depleted cells, RhoB levels were similarly increased by both drugs (Figure S3—figure supplement 3C and 3D), indicating that both the proteasomal and the endo-lysosomal pathway are involved in RhoB protein degradation in cells with Solo downregulation.

In sum, these experiments show that Solo and DLC3 form a novel GEF—GAP pair that regulate endosomal RhoB in a complex manner,

modulating not only its total cellular activity, but also its localization and turnover rates.

3.5 | Solo regulates EGFR trafficking and signalling

We previously found DLC3 to control EGFR degradation, a receptor tyrosine kinase that is rapidly endocytosed upon EGF ligand binding and is transported to the lysosomes in a RhoB-dependent manner.[14,39,40] Considering the functional connection between Solo and DLC3, we explored whether Solo is also required for the regulation of EGFR trafficking. To this end, HeLa cells were stimulated with EGF and subjected to immunofluorescence staining with an antibody recognizing the extracellular part of EGFR. This was followed by permeabilization and incubation with an antibody binding to the intracellular domain of the receptor, enabling us to visualize surface and total EGFR pools (Figure 4A and Figure S4—figure supplement 1). These experiments revealed a stabilization of EGFR in the Solo knockdown cells. Because the receptor trafficking route determines the signalling response we next examined activation of the EGFR and downstream pathways by immunoblotting. Consistent with the immunofluorescence studies, Solo knockdown cells displayed increased basal EGFR levels and maintained elevated levels of the receptor for longer times post EGF stimulation (Figure 4B,C). Interestingly, in spite of EGFR phosphorylation (Figure 4D), downstream activation of the MAPK and PI3K pathways was dampened in Solo knockdown cells, as measured by AKT (Figure 4E) and ERK phosphorylation (Figure 4F), respectively. This indicates that EGFR cannot engage in efficient signalling under

FIGURE 2 Solo activates RhoB on endosomes. (A) HEK293T cells were co-transfected with plasmids encoding for HA-Solo and the indicated GFP-RhoB variants. A plasmid encoding for empty GFP served as a negative control. 24 h post transfection the lysates were analysed directly (input) or used for GFP-Trap assays followed by immunoblotting with the indicated antibodies. (B) Representative confocal immunofluorescence microscopy images of HeLa cells transiently expressing GFP-RhoB 19N (green) and HA-Solo (red). Images show one confocal plane and were acquired using the superresolution modus of the Airyscan device. (C) Representative confocal immunofluorescence microscopy images of HeLa cells transiently expressing GFP-RhoA 19N (green) and HA-Solo (red). Images show one confocal plane and were acquired using the superresolution modus of the Airyscan device. (D) ImageJ was used to quantify the Manders' overlap coefficient for HA-Solo with RhoA/B in images representatively shown in (B) and (C). The box plot shows the results of three independent experiments, where each dot represents one cell. Centre lines show the medians; box limits indicate the 25th and 75th percentiles as determined by GraphPad Prism 7 software; whiskers extend 1.5 times the interquartile range from the 25th and 75th percentiles, outliers are represented by dots. $N = 49$ (RhoA19N) and 41 (RhoB19N); $n = 3$. Significance was determined via unpaired t-test, ****$p < 0.0001$. (E) Schematic representation of the optogenetic experimental workflow employed to monitor endosomal RhoB activation upon Solo-GEF recruitment. See text for details. (F) 6 h post transfection with the constructs described in (E), HeLa cells were exposed to 488-nm light and imaged. Shown are representative confocal microscopy images, illustrating the enrichment of the GFP-AHPH Rho-GTP reader (green) to sites of OptoEndo-Solo-GEF (red) recruitment. The GFP-AHPH A70D/E758K mutant (GFP-AHPH*) was used as a negative control. All images were acquired and are displayed with the same settings. Images show one confocal plane. Scale bar: 5 μm. (G) Quantification of the GFP-AHPH recruitment experiment shown in (D). The box plot shows the results of three independent experiments, where each dot represents one mCherry positive endosome. Centre lines show the medians; box limits indicate the 25th and 75th percentiles as determined by GraphPad Prism 7 software; whiskers extend 1.5 times the interquartile range from the 25th and 75th percentiles, outliers are represented by dots. $N = 30$ cells; $n = 3$, with more than 600 vesicles analysed per condition. The significance of differences was analysed by Mann–Whitney t-test; ****$p \leq 0.0001$, n.s.: non-significant. (H) Quantification of the GFP-AHPH recruitment to OptoEndo-Solo GEF endosomes in HeLa cells transfected with either control (siNT) or with RhoB siRNAs (siRhoBsp left and siRhoBss, right). The box plot shows the results of three independent experiments, where each dot represents one cell. Centre lines show the medians; box limits indicate the 25th and 75th percentiles as determined by GraphPad Prism 7 software; whiskers extend 1.5 times the interquartile range from the 25th and 75th percentiles, outliers are represented by dots. $N = 26–30$ cells; $n = 3$. Statistical significance was determined by unpaired t-test with Welch's correction, *$p \leq 0.05$. See also Figure S2—figure supplement 1. For statistical testing data, see Table S2
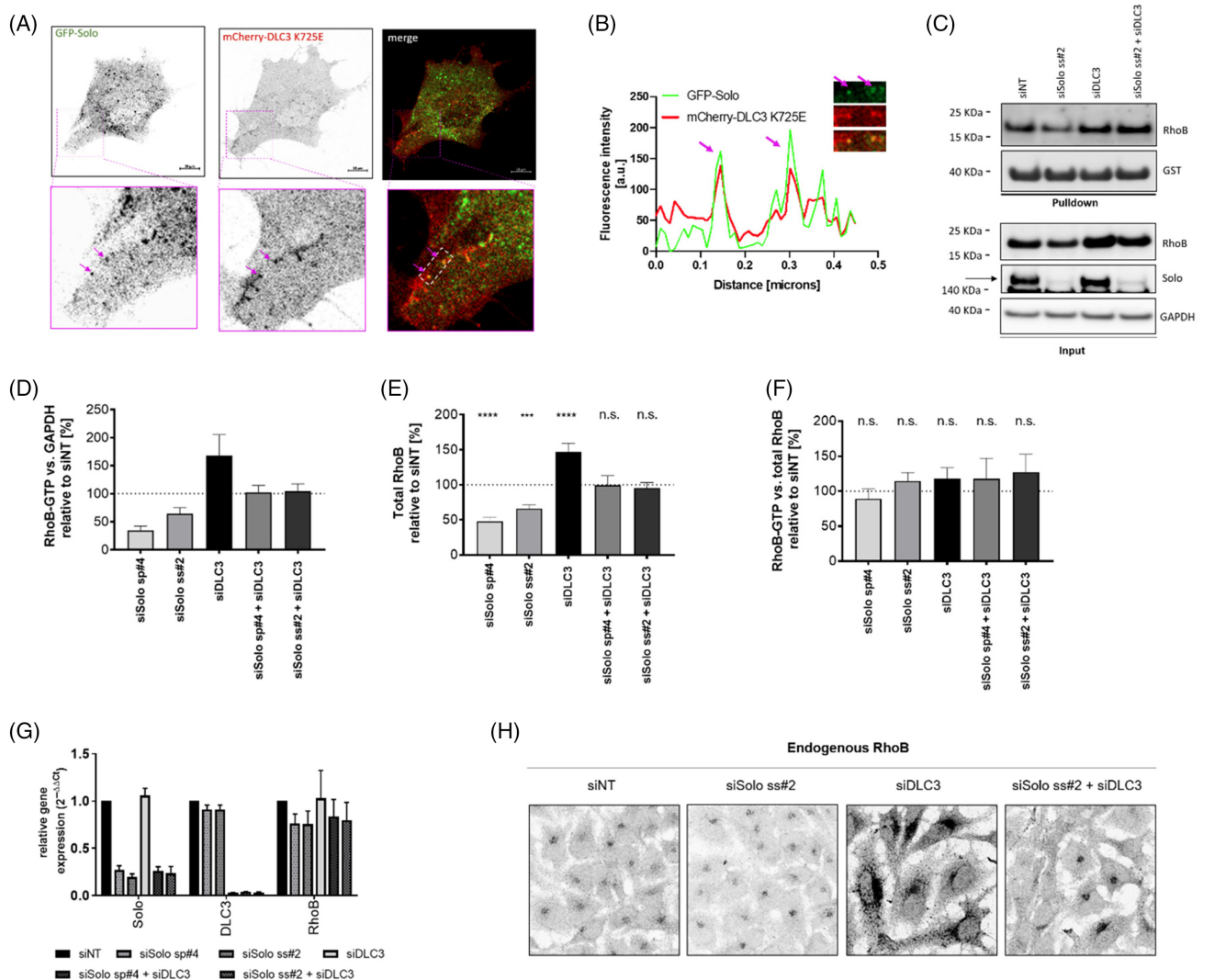
FIGURE 3 Solo and DLC3 co-regulate RhoB activity and protein levels. (A) HeLa cells were transiently transfected with plasmids encoding GFP-Solo and mCherry-DLC3 K725E followed by imaging 24 h later. Shown is a selected time frame from the live cell imaging experiment. Arrows highlight exemplary areas of colocalization between the two fluorescently tagged proteins. Images display a single confocal section. Scale bar: 10 μm. See also Movie S1. (B) Intensity profiles of GFP-Solo (green) and mCherry-DLC3 K725E (red) extracted in ImageJ along a straight line crossing the white rectangle annotated in (A). Arrows highlight exemplary areas of colocalization between the two fluorescently tagged proteins. (C) HeLa cells were transfected with the indicated siRNAs. At 72 h post knockdown, the cells were stimulated with 100 ng/ml EGF for 5 min, followed by lysis and GST–RBD pulldown assays. Pulldowns and total cell lysates were analysed by immunoblotting with the indicated antibodies. The band corresponding to Solo is annotated with an arrow. (D–F) Western blots from the experimental set representatively shown in C were quantified using the ImageQuant TL software. (D) The RhoB-GTP pulldown signal was normalized to GAPDH and further divided by the signal obtained for the siNT sample. The value obtained for the siNT control was set as 100%, marked with the dotted line. (E) The total RhoB signal in the input was normalized to GAPDH and further divided by the signal obtained for the siNT sample. The value obtained for the siNT control was normalized to 100%, marked with the dotted line. (F) The RhoB-GTP pulldown signal was normalized to total RhoB and GAPDH and further divided by the signal obtained for the siNT sample. The value obtained for the siNT control was set as 100%, marked with the dotted line. The significance of differences was analysed by a one-way ANOVA and Dunett post-test; Control is the siNT sample. The significance of differences was analysed by a one-way ANOVA and Dunett post-test; ****$p \le 0.0001$; ***$p \le 0.0002$, n.s.: non-significant. Control is the siNT sample. $n = 3$–5. (G) qRT-PCR measurements of the Solo, DLC3 and RhoB transcripts in HeLa cells subjected to knockdown with the indicated siRNAs. RNA was isolated at 72 h post transient transfection. Gene expression values were normalized to the reference gene RPLP0. Shown is the relative change of each transcript normalized to the corresponding siNT sample, which was set to 1. $n = 3$, error bars: SEM. (H) HeLa cells were transfected with the indicated siRNAs. At 72 h post knockdown, the cells were fixed and stained for RhoB. Shown are representative maximum intensity projections of five confocal sections. All images were acquired and displayed using identical settings. See also Figure S3—figure supplements 1–3. For statistical testing data, see Table S2
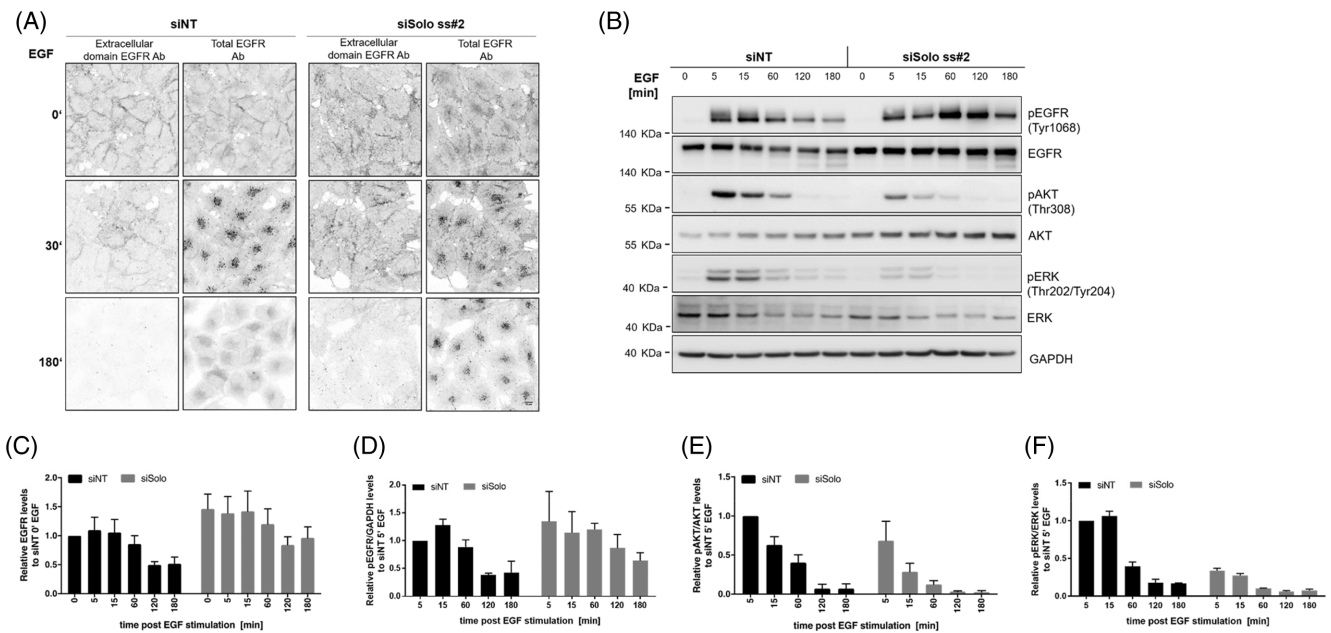
FIGURE 4 Solo knockdown delays epidermal growth factor receptor (EGFR) trafficking and dampens the EGF signalling response. (A) HeLa cells were transiently transfected with control (siNT) or Solo-specific (siSolo ss#2) siRNAs. Following a 48 h incubation period, the cells were serum starved overnight and, prior to fixation, stimulated with 10 ng/mL EGF for the indicated times. The cells were then stained with an antibody recognizing the extracellular domain of EGFR (surface EGFR). This was followed by permeabilization and immunostaining with an antibody recognizing the C-terminal part of EGFR (total EGFR). Shown are representative maximum intensity projections of five confocal sections. All images were acquired and displayed using identical settings. Scale bar: 10 μm. (B) Following knockdown and EGF stimulation as described in (A), HeLa cells were lysed, followed by immunoblotting with the indicated antibodies. The shown experiment is representative of three independent biological repeats. (C) Densitometric quantification of total EGFR levels in siNT and siSolo cells of the EGF stimulation experiment representatively shown in (B). EGFR levels of the different time points were normalized to GAPDH and subsequently divided by the signal measured for the unstimulated siNT cells, which was set to 1. (D) Densitometric quantification of pEGFR levels in siNT and siSolo cells of the EGF stimulation experiment representatively shown in (B). pEGFR levels of the different time points were normalized to GAPDH and subsequently divided by the signal measured for the siNT cells at 5 min post EGF stimulation, which was set to 1. (E) Densitometric quantification of the pAKT-Thr308 levels in siNT and siSolo cells of the EGF stimulation experiment representatively shown in (B). The phosphorylation signal was normalized to the one obtained for the unphosphorylated protein and GAPDH and subsequently divided by the signal measured for the siNT cells at 5 min post EGF stimulation. The value obtained for the siNT cells was further normalized to 1. (F) Densitometric quantification of the pERK (Thr202/Tyr204) levels in siNT and siSolo cells of the EGF stimulation experiment representatively shown in (B). The phosphorylation signal was normalized to the one obtained for the unphosphorylated protein and GAPDH and subsequently divided by the signal measured for the siNT cells at 5 min post EGF stimulation. The value obtained for the siNT cells was further normalized to 1. (C–F) The bar diagrams display the mean values of three independent biological repeats, cumulating two experiments using siSolo ss#2 and one experiment using siSolo sp#4. Error bars: SEM. See also Figure S4—figure supplement 1. For statistical testing data, see Table S2

these conditions, presumably resulting from EGFR mislocalization and the absence of respective downstream effector molecules.

In sum, our experiments identify Solo—DLC3 as a functionally connected GEF—GAP pair that regulates RhoB and endocytic trafficking, impinging on cellular signalling responses triggered by EGF.

4 | DISCUSSION

Understanding how GEF and GAPs coordinately control Rho GTPase signalling in a precise spatiotemporal manner is a long-standing challenge. In this study, we established an unbiased microscopy RNAi screen using the Golgi complex as a sensor and identified Solo as a RhoGEF protein that counteracts the cellular activity of DLC3. We further discovered that the interplay between Solo and DLC3 is

pivotal to the regulation of RhoB, a GTPase of central importance for endocytic trafficking.

Solo was previously described as a RhoA/C-targeting GEF involved in mechanotransduction, by binding and organizing keratin-8/keratin-18 (K8/K18) filaments, thereby mediating force-induced RhoA activation and stress fibre formation.[28,41,42] Here, we uncover a previously unknown function of Solo in maintaining the integrity of the Golgi complex. Both the actin and microtubule cytoskeleton play a major role in the structure, function and positioning of the Golgi complex.[25,26] In addition, a few studies also suggest that an intact keratin network is required for the maintenance of Golgi structure.[42–44] While our work did not focus on the organization of cytokeratin filaments, we did find that Solo depletion reduces stress fibre formation in HeLa cells (Figure S1—figure supplement 1E), indicating that the Golgi phenotype we observe here may be a consequence of

cytoskeletal rearrangements downstream of altered Rho activity. Importantly, out of the 23 RhoGEFs we tested in our imaging-based screen, Solo stood out for its ability to antagonize the fragmented Golgi phenotype caused by DLC3 depletion. This provides strong evidence that the effect of Golgi morphology is specifically downstream of the Solo—DLC3 interplay and not an unspecific readout of globally perturbed RhoGEF—RhoGAP balance.

In addition to the actin cytoskeleton, the morphology of the Golgi complex is also influenced by membrane trafficking homeostasis. Among GTPases, in particular, RhoA, RhoB, RhoD, Rac and Cdc42 have been shown to affect various steps of membrane trafficking. Interestingly, while the GEF activity was important for the Golgi compaction phenotype, Solo was not enriched at this organelle under steady state. The localization of Solo on a subset of RhoB positive endosomes rather suggests that the effects on Golgi morphology could also stem from altered membrane trafficking. Notably, the GEF activity of Solo appeared to be important for the vesicular localization of Solo since the GEF inactive mutant displayed a diffuse cytoplasmic distribution. This hints at a positive feedback loop between Solo activation and membrane enrichment. Such a mechanism was previously reported for the Sec7 Arf-GEF at the TGN.[45] This GEF-dependent change in the vesicular localization of Solo was also observed in HUVEC cells,[28] suggesting that the involvement of Solo in endocytic trafficking is conserved in other cellular systems as well. In line with this, Solo was contained in the endosomal mass spectrometry dataset of MEF cells obtained by Ivaska and co-workers.[46] While these studies do not allow to discriminate whether Solo is an endosomal cargo or an activator of RhoB, our optogenetic approach enabled us to address endosomal RhoB activation by Solo-GEF in a localized manner. To our knowledge, this is the first report of a direct readout of endogenous endosomal RhoB activation. Although we cannot exclude that Solo impinges on Golgi complex structure by regulation of RhoA as well, our study clearly demonstrates a role of Solo in the regulation of RhoB. Since most of the endogenous Solo is membrane attached, for the future it will be interesting to explore the cellular cues that regulate the activation of full-length Solo on endomembranes.

We further uncover a multifactorial involvement of Solo and DLC3 in the regulation of RhoB, which extends beyond the regulation of its Rho GTPase activity. Specifically, we find that the interplay between Solo and DLC3 controls the activity, the subcellular distribution as well as the total protein levels of RhoB. Although we were not able to pinpoint the mechanistic details responsible for RhoB protein level regulation, an intact endosomal trafficking system was recently found to be required for the homeostasis of cellular RhoB amounts and protein localization.[30,34] This indicates that Solo and DLC3 may not only control RhoB activity directly, but also indirectly by impinging on the endocytic recycling compartment.

Motivated by the interplay between Solo and RhoB, we also investigated the role of Solo in EGFR signalling and trafficking. Mirroring the effects of DLC3 depletion,[14] Solo knockdown dampened AKT activation in response to EGF stimulation. These results indicate that the cellular levels of Solo play a critical role in determining the trafficking route of EGFR, hence the signalling potency of the receptor. The exact molecular mechanism behind this effect is, however, still open. Impairment of EGFR endocytosis using a dominant-negative dynamin mutant dampens PI3K/AKT and ERK signalling, leading to inhibition of EGF-dependent mitogenesis.[47] This is in line with our microscopy studies in HeLa cells where we observed delayed EGFR internalization and signalling upon Solo knockdown. The fact that both Solo and DLC3 knockdown delay EGFR trafficking while leading to opposing downstream signalling outcomes, illustrates the delicate GEF—GAP balance that is in place to control the trafficking and signalling capacity of this receptor. Besides the EGFR, it is plausible that also other cargoes are regulated by Solo and DLC3. For the future, it would be interesting to identify these through a more global approach. This strategy is expected to deliver insights into the cellular processes that are commonly regulated by Solo and DLC3, plus additional functions the two proteins might have that are independent of each other.

CONFLICT OF INTEREST

The authors declare no competing or financial interests.

DATA AVAILABILITY STATEMENT

Data generated or analyzed during this study are included in the manuscript and supporting files: The siRNA sequences included in the RhoGEF library are provided in Table S1. The *p* values for the Golgi screen are displayed in Figure S2. *p* Values for all other statistical tests are provided in Table S2. The raw data of the Golgi screen, Table S3, is available from University of Stuttgart at: https://darus.uni-stuttgart.de/privateurl.xhtml?token=e0aa3f7b-ac8c-4253-8eb4-c8ae826346eb. This study generated the following new plasmids: pIRESNEO-Solo L1217E-HA, pEGFP-RhoB T19N and CRY2-Solo-

GEF-mCherry. Plasmids generated in this study as well as the anti-Solo antibody are available upon reasonable request. Further information and requests for plasmids, resources and reagents should be directed to the lead contact Monilola A. Olayioye.

ORCID

Cristiana Lungu [ORCID] https://orcid.org/0000-0003-4021-1841
Marcel Hörning [ORCID] https://orcid.org/0000-0001-8934-048X
Monilola A. Olayioye [ORCID] https://orcid.org/0000-0003-1093-263X

REFERENCES

1. Anitei M, Hoflack B. Bridging membrane and cytoskeleton dynamics in the secretory and endocytic pathways. *Nat Cell Biol*. 2011;14:11-19.
2. Olayioye MA, Noll B, Hausser A. Spatiotemporal control of intracellular membrane trafficking by Rho GTPases. *Cell*. 2019;8:1478.
3. Phuyal S, Farhan H. Multifaceted Rho GTPase signaling at the endomembranes. *Front Cell Dev Biol*. 2019;7:127.
4. Bos JL, Rehmann H, Wittinghofer A. GEFs and GAPs: critical elements in the control of small G proteins. *Cell*. 2007;129:865-877.
5. Vigil D, Cherfils J, Rossman KL, Der CJ. Ras superfamily GEFs and GAPs: validated and tractable targets for cancer therapy? *Nat Rev Cancer*. 2010;10:842-857.
6. Adamson P, Paterson HF, Hall A. Intracellular localization of the P21rho proteins. *J Cell Biol*. 1992;119:617-627.
7. Wherlock M, Gampel A, Futter C, Mellor H. Farnesyltransferase inhibitors disrupt EGF receptor traffic through modulation of the RhoB GTPase. *J Cell Sci*. 2004;117:3221-3231.
8. Zilberman Y, Alieva NO, Miserey-Lenkei S, et al. Involvement of the Rho-mDia1 pathway in the regulation of Golgi complex architecture and dynamics. *Mol Biol Cell*. 2011;22:2900-2911.
9. Aspenström P. Fast-cycling Rho GTPases. *Small GTPases*. 2020;11:248-255.
10. Braun AC, Olayioye MA. Rho regulation: DLC proteins in space and time. *Cell Signal*. 2015;27:1643-1651.
11. Fritz RD, Pertz O. The dynamics of spatio-temporal Rho GTPase signaling: formation of signaling patterns. *F1000Res*. 2016;5:749.
12. Kandpal RP. Rho GTPase activating proteins in cancer phenotypes. *Curr Protein Pept Sci*. 2006;7:355-365.
13. Xue W, Krasnitz A, Lucito R, et al. DLC1 is a chromosome 8p tumor suppressor whose loss promotes hepatocellular carcinoma. *Genes Dev*. 2008;22:1439-1444.
14. Braun AC, Hendrick J, Eisler SA, Schmid S, Hausser A, Olayioye MA. The Rho-specific GAP protein DLC3 coordinates endocytic membrane trafficking. *J Cell Sci*. 2015;128:1386-1399.
15. Noll B, Benz D, Frey Y, et al. DLC3 suppresses MT1-MMP-dependent matrix degradation by controlling RhoB and actin remodeling at endosomal membranes. *J Cell Sci*. 2019;132:jcs223172.
16. Finney DJ. On the distribution of a variate whose logarithm is normally distributed. *J R Stat Soc*. 1941;7:155.
17. Tei R, Baskin JM. Spatiotemporal control of phosphatidic acid signaling with optogenetic, engineered phospholipase Ds. *J Cell Biol*. 2020;219:e201907013.
18. Valon L, Marín-Llauradó A, Wyatt T, Charras G, Trepat X. Optogenetic control of cellular forces and mechanotransduction. *Nat Commun*. 2017;8:14396.
19. Holeiter G, Bischoff A, Braun AC, et al. The RhoGAP protein Deleted in Liver Cancer 3 (DLC3) is essential for adherens junctions integrity. *Oncogenesis*. 2012;1:e13.
20. Piekny AJ, Glotzer M. Anillin is a scaffold protein that links RhoA, actin, and myosin during cytokinesis. *Curr Biol*. 2008;18:30-36.
21. Priya R, Gomez GA, Budnar S, et al. Feedback regulation through myosin II confers robustness on RhoA signalling at E-cadherin junctions. *Nat Cell Biol*. 2015;17:1282-1293.
22. Bolte S, Cordelières FP. A guided tour into subcellular colocalization analysis in light microscopy. *J Microsc*. 2006;224:213-232.
23. Tinevez J-Y, Perry N, Schindelin J, et al. TrackMate: an open and extensible platform for single-particle tracking. *Methods*. 2017;115:80-90.
24. Linkert M, Rueden CT, Allan C, et al. Metadata matters: access to image data in the real world. *J Cell Biol*. 2010;189:777-782.
25. Egea G, Serra-Peinado C, Salcedo-Sicilia L, Gutiérrez-Martínez E. Actin acting at the Golgi. *Histochem Cell Biol*. 2013;140:347-360.
26. Yadav S, Linstedt AD. Golgi Positioning. *Cold Spring Harb Perspect Biol*. 2011;3:a005322.
27. Bard F, Mazelin L, Péchoux-Longin C, Malhotra V, Jurdic P. Src regulates Golgi structure and KDEL receptor-dependent retrograde transport to the endoplasmic reticulum. *J Biol Chem*. 2003;278:46601-46606.
28. Abiko H, Fujiwara S, Ohashi K, et al. Rho guanine nucleotide exchange factors involved in cyclic-stretch-induced reorientation of vascular endothelial cells. *J Cell Sci*. 2015;128:1683-1695.
29. Jia R, Bonifacino JS. Lysosome positioning influences mTORC2 and AKT signaling. *Mol Cell*. 2019;75:26-38.e3.
30. Gong X, Didan Y, Lock JG, Strömblad S. KIF13A-regulated RhoB plasma membrane localization governs membrane blebbing and blebby amoeboid cell migration. *EMBO J*. 2018;37:e98994.
31. Raiborg C, Schink KO, Stenmark H. Class III phosphatidylinositol 3-kinase and its catalytic product PtdIns3P in regulation of endocytic membrane traffic. *FEBS J*. 2013;280:2730-2742.
32. Canguilhem B, Pradines A, Baudouin C, et al. RhoB protects human keratinocytes from UVB-induced apoptosis through epidermal growth factor receptor signaling. *J Biol Chem*. 2005;280:43257-43263.
33. Kamon H, Kawabe T, Kitamura H, et al. TRIF-GEFH1-RhoB pathway is involved in MHCII expression on dendritic cells that is critical for CD4 T-cell activation. *EMBO J*. 2006;25:4108-4119.
34. Zaoui K, Rajadurai CV, Duhamel S, Park M. Arf6 regulates RhoB subcellular localization to control cancer cell invasion. *J Cell Biol*. 2019;218:3812-3826.
35. Engel ME, Datta PK, Moses HL. RhoB is stabilized by transforming growth factor beta and antagonizes transcriptional activation. *J Biol Chem*. 1998;273:9921-9926.
36. Lebowitz PF, Davide JP, Prendergast GC. Evidence that farnesyltransferase inhibitors suppress Ras transformation by interfering with Rho activity. *Mol Cell Biol*. 1995;15:6613.
37. Kovačević I, Sakaue T, Majoleé J, et al. The Cullin-3-Rbx1-KCTD10 complex controls endothelial barrier function via K63 ubiquitination of RhoB. *J Cell Biol*. 2018;217:1015-1032.
38. Pérez-Sala D, Boya P, Ramos I, Herrera M, Stamatakis K. The C-terminal sequence of RhoB directs protein degradation through an endo-lysosomal pathway. *PLoS One*. 2009;4:e8117.
39. Gampel A, Parker PJ, Mellor H. Regulation of epidermal growth factor receptor traffic by the small GTPase RhoB. *Curr Biol*. 1999;9:955-958.
40. Tomas A, Futter CE, Eden ER. EGF receptor trafficking: consequences for signaling and cancer. *Trends Cell Biol*. 2014;24:26-34.
41. Curtis C, Hemmeryckx B, Haataja L, Senadheera D, Groffen J, Heisterkamp N. Scambio, a novel guanine nucleotide exchange factor for Rho. *Mol Cancer*. 2004;3:10.
42. Fujiwara S, Ohashi K, Mashiko T, Kondo H, Mizuno K. Interplay between Solo and keratin filaments is crucial for mechanical force-induced stress fiber reinforcement. *Mol Biol Cell*. 2016;27:954-966.
43. Kumemura H, Harada M, Omary MB, et al. Aggregation and loss of cytokeratin filament networks inhibit golgi organization in

liver-derived epithelial cell lines. *Cell Motil Cytoskeleton*. 2004;57: 37-52.

44. Marceau N, Loranger A, Gilbert S, Daigle N, Champetier S. Keratin-mediated resistance to stress and apoptosis in simple epithelial cells in relation to health and disease. *Biochem Cell Biol*. 2001;79:543-555.

45. Richardson BC, Fromme JC. Autoregulation of Sec7 Arf-GEF activity and localization by positive feedback. *Small GTPases*. 2012;3: 240-243.

46. Alanko J, Mai A, Jacquemet G, et al. Integrin endosomal signalling suppresses anoikis. *Nat Cell Biol*. 2015;17:1412-1421.

47. Vieira AV, Lamaze C, Schmid SL. Control of EGF receptor signaling by clathrin-mediated endocytosis. *Science*. 1996;274:2086-2089.

SUPPORTING INFORMATION

Additional supporting information can be found online in the Supporting Information section at the end of this article.